Received: 19 October 2021 | Accepted: 25 February 2022

DOI: 10.1002/maco.202112871

ARTICLE

Materials and Corrosion

Marine atmospheric corrosion of carbon steel in the tropical microclimate of Port Louis

Yashwantraj Seechurn[1,2] | Baboo Y. R. Surnam[1] | Julian A. Wharton[2]

[1]Mechanical and Production Engineering Department, Faculty of Engineering, University of Mauritius, Réduit, Moka, Mauritius

[2]School of Engineering, National Centre of Advanced Tribology at Southampton (nCATS), University of Southampton, Southampton, Hampshire, UK

Correspondence
Yashwantraj Seechurn, Mechanical and Production Engineering Department, Faculty of Engineering, University of Mauritius, Réduit 80837, Mauritius.
Email: yashwantrajseechurn@yahoo.com

Abstract

The atmospheric corrosion performance of S235 carbon steel is assessed when exposed to the tropical/marine aerosol pollutants of Port Louis, Mauritius. Port Louis is situated on the northwest coast and has a distinct microclimate, leading to major atmospheric corrosion concerns. In addition, sulphur dioxide emissions from three heavy oil-fired power stations complicate corrosion prediction within the region. Mass-loss analysis shows distinctive corrosion progression behaviours linked to the environmental and geographical variables. The formation of porous surface layers leads to a continuous increase in metal dissolution during the electrochemical process. The surface analysis reveals lepidocrocite (γ-FeOOH) and goethite (α-FeOOH) as the predominant rust phases, with low percentages of magnetite (Fe_3O_4), akageneite (β-FeOOH) and jarosite ($KFe_3(OH)_6(SO_4)_2$). A key insight in the S235 atmospheric corrosion involves two stages: the early rapid corrosion stage followed by a slow stage of linear or power-law corrosion kinetics due to the formation of stable rust phases.

KEYWORDS

atmospheric corrosion, carbon steel, rust, SEM, weight loss, X-ray diffraction

1 | INTRODUCTION

Atmospheric corrosion is known to be severe in coastal zones worldwide; however, the mechanism of corrosion in atmospheres associated with high humidity, airborne natural marine aerosols and heavy industry contaminants is not fully understood.[1] Carbon steels are by far the most important, multifunctional and most adaptable structural material. Corrosion management strategies for carbon steels are essential to maximise the resilience of all manners of sustainable infrastructure development, especially for countries with emerging/small economies such as Mauritius. Characterisation of the dominant environmental parameters, such as the temperature-humidity complex, airborne chloride levels and sulphur dioxide are key to establishing corrosivity estimates. The actual corrosion rates in coastal environments can be difficult to predict due to variable chloride deposition rates. Likewise, sulphur dioxide plays an important role in atmospheric corrosion of steel infrastructure in urban and industrial areas, leading to the formation of sulphur compounds, such as rozenite, melanterite and jarosite.[2,3]

Mauritius is a small island (land area: 1865 km^2) with 330 km of coastline and is situated 865 km east of Madagascar (Figure 1). It has a tropical climate with abundant rainfall (2010 mm annually), high humidity levels (mainly above 80%) and only two seasons: winter and summer.[4] The island is also under the influence of

steady south-easterly trade winds (Figure 2) carrying natural airborne sea aerosols inland. All these environmental conditions combined, lead to atmospheric corrosion with deleterious effects on infrastructure, particularly in the coastal regions of the island.

Coastal atmospheric corrosion is of particular concern for Port Louis (PL) (20.2°S, 57.5°E), the harbour and capital city on the north-west coast, with an industrial zone comprising three power plants, namely Saint-Louis, Fort-Victoria and Fort George (FG), of 100, 107 and 134 MW total effective capacity, respectively.[5] The power stations generate electricity from the combustion of heavy fuel oil and are large emitters of gases, such as SO_2 and NO_x among others. In 2016, stack gases of 16157 mg m^{-3} NO_2 and 6537 mg m^{-3} SO_2 contents were released from FG.[6] The presence of natural atmospheric marine aerosols coupled with anthropogenic contaminants/ pollution from power industries makes the atmospheric conditions in PL distinct from the conditions prevailing over the rest of the island. Major salinity differences may also exist between the shores of one side of a country and the other side as each region varies in terms of its characteristics pertaining to the corrosion behaviour of materials.[7] In Mexico, for example, the corrosion rate for the northern coast is 362.4 μm annum^{-1} (μm a^{-1}), which is significantly higher than the corrosion rate of 91.3 μm a^{-1} obtained for the southern coast.[8]

In addition, PL is situated on the leeward side of the Moka mountain range (Figure 2), which contributes to its microclimate, hindering the prevailing rain patterns, causing the land to remain dry and producing less moisture in the air.[9] Atmospheric corrosion data from a previous study undertaken at a specific location within PL have shown that the region is highly corrosive.[10] However, given the spatial variability of atmospheric conditions in PL, corrosivity estimates determined from a single exposure location are not necessarily representative of the wider region. Moreover, the environmental conditions prevailing at other island locations are not similar to those of PL. Therefore, this study uses additional outdoor exposures to obtain a more comprehensive corrosivity assessment of PL, for more effective long-term corrosion prediction, by determining the nature of rust layers and the mechanism of transformation from one phase to another.[11] Similar investigations have often utilised SEM and XRD for the analysis and characterisation of corrosion products on metallic surfaces.[12–15] However, the data available on the specific morphology of rust phases, with

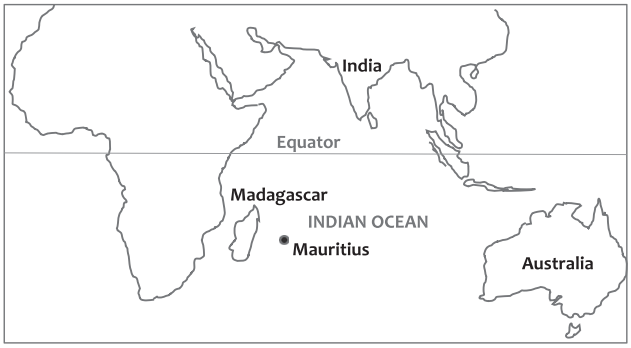

FIGURE 1 Map showing Mauritius in the Indian Ocean

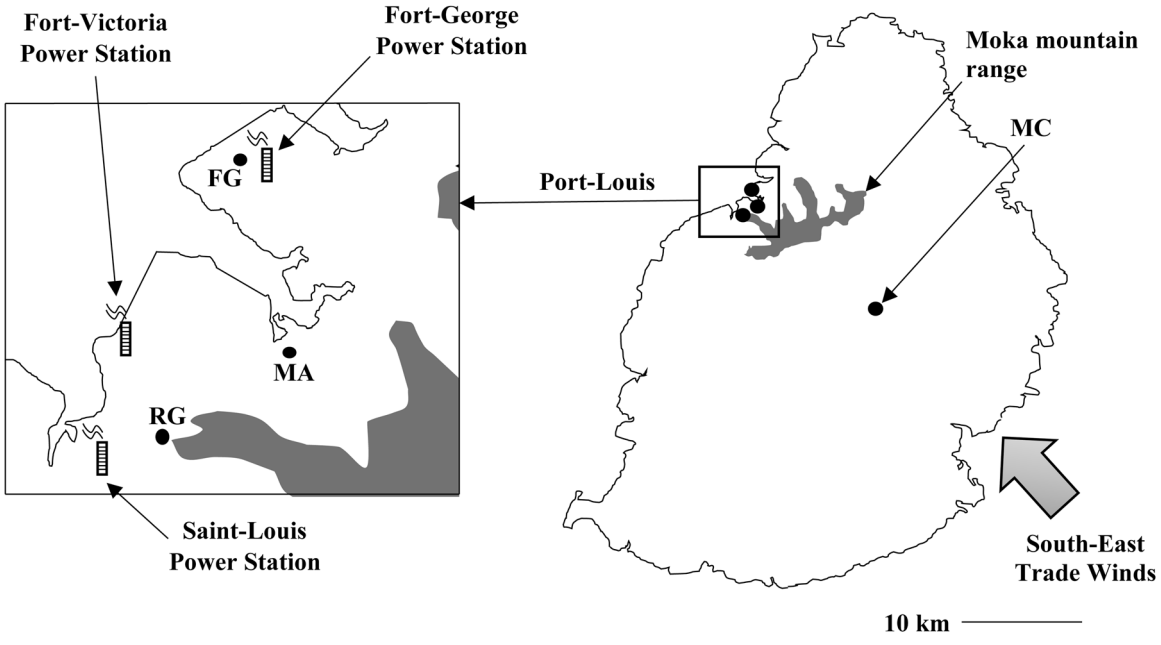

FIGURE 2 Map of Mauritius and Port Louis showing critical locations and test sites

respect to identified chemical components within the corroded layers is limited. As such, morphologies associated with rust phases need to be justified by determining the specific formation mechanism in the prevailing environment.

2 | MATERIALS AND METHODS/ EXPERIMENTAL

2.1 | Field exposure

To determine the atmospheric corrosion performance of S235 carbon steel, three sites (Figure 2) were selected in PL, namely Fort George (FG), Rajiv Gandhi (RG) and Mutual Aid (MA), having elevations above sea level of 8, 41 and 11 m, respectively. Moreover, a control atmosphere (Medine Camp de Masque—MC), around 283 m above sea level, was also considered as shown in Figure 2. FG is 50 m downwind of a heavy-oil power plant chimney and 350 m inland from the coast. It has the characteristics of a marine-heavy industrial environment. Sulphur dioxide (SO_2) emissions from the combustion of heavy fuel oil are likely to be the main contributor to corrosion in this area, with sulphate aerosols also expected to naturally occur due to the photooxidation of dimethylsulphide present in seawater (accounting for approximately 50% of the total biogenic sulphur flux to the atmosphere, and linked to diurnal and annual variations).[16] MA, situated in the city centre, is 203 m from the coastline and pollutants in the atmosphere are representative of a marine-urban environment. RG is situated away from the city centre but close to an industrial zone, comprising a power station and other industries. Data collected from this site should give an indication of the influence of marine salts on metal surfaces exposed in the outskirts of PL and at a distance (896 m) further away from the coast. MC is a rural area located 17 km from the east coast, closer to the island centre and upwind from any industrial pollutants. The prevailing south-easterly trade winds mean that the MC atmosphere will not be free from exposure to either chlorides (Cl^-) or SO_2.

Deposition rates of Cl^- and SO_2 levels in the atmosphere were determined by the wet candle method and lead oxide sulfation plates (shown in Appendix), respectively, as per ISO 9225.[17] Two monthly measurements, each involving a single wet candle and two sulfation plates, were taken in each season (winter and summer) to determine seasonal variation. The Cl^- and SO_2 concentrations obtained using the mercuric thiocyanate method and a turbidimetric method, respectively, were validated using a standard solution.[17] Bare S235 carbon steel plates, with the composition shown in Table 1, having the surface roughness measure Ra of 4.2 μm and dimensions of 150 mm × 100 mm × 3 mm, were exposed to the atmosphere in appropriate racks according to ISO 8565[18] from June 2018 to June 2019. The expected main corroding source at PL being the sea salt aerosol, all the racks were facing the ocean, while the rack at MC was oriented towards the north (Supplementary Information: Appendix). Before exposure, the metal plates were immersed in a solution of 10% wt./vol. hydrochloric acid (HCl specific gravity 1.19) to remove the mill scale and oxides from the surface. The pickled plates were rinsed thoroughly with distilled water, hot air-dried using a specimen dryer and then stored in a desiccator. Removal of quintuplicate plates were carried out at each test site after 2, 5, 8 and 11 months of exposure. From the five plates at each time point, two were used for corrosion product characterisation (optical/electron microscopy and X-ray diffraction [XRD]) and the remaining three were taken for mass-loss analysis as per ISO 8407.[19] Each plate was weighed to three decimal places using the Kern precision balance PB 400-3.

TABLE 1 Chemical composition of the S235 carbon steel

Steel	C	Mn	P	S	Si	Cu
S235	0.17	1.4	0.04	0.04	0.05	0.55

2.2 | Corrosion rate determination

The corrosion rate (r_{corr}) was calculated as per ISO 9226 using the following Equation (1): [20]

$$r_{corr} = \frac{\Delta m}{At}, \quad (1)$$

where Δm is the mass loss in g, A is the surface area in m^2, and t is the exposure time in years (a).

It is well known that r_{corr} does not remain constant after the initial stages of surface degradation since the accumulation of corrosion products with time leads to a decrease in corrosion rate, depending on the nature of the rust phases. However, r_{corr}, which is often determined from first-year data, can also be used to estimate the corrosion deterioration (plate thickness loss) for long-term exposures.[21] According to ISO 9224, 'total attack' (D), assessed using Equation (2), is useful for approximating the progress of corrosion damage.[22] The exponent b is a complex association of the type of atmosphere, the variation of climatic factors such as time-of-wetness and any other prevailing conditions at the exposure site. Equation (2) is similar to the established expression of the form $M = at^b$, where M is the mass loss, t is the number of exposure years with a and b being constants.[23] A b value around 0.5 suggests that the atmosphere is mildly polluted, whereas b greater than 1 represents a coastal

region irrespective of the concentration of chloride. Specific values of r_{corr} and b obtained for each material and the associated environment could be used to determine D for extended exposures.[24–26]

$$D = r_{corr} t^b, \quad (2)$$

where t represents years of exposure (a), r_{corr} is the corrosion rate in $g\,m^{-2}\,a^{-1}$ and b is a time exponent indicative of the metal and environment.

In addition to corrosion rate, climate and pollution parameters, such as airborne salinity and SO_2 levels, were also used in categorising the atmospheric environments based on a corrosivity classification method provided in ISO 9223.[27] The weather information used in this study, such as monthly rainfall, wind direction and mean monthly wind speed, relative humidity (RH) and temperature, are all quality controlled observed data provided by the Mauritius Meteorological Services and also derived from monthly Meteorological Observations and Climatological Summaries.[28] A parameter often used instead of RH is time-of-wetness (TOW), defined in ISO 9223 as the time during which RH exceeds 80% and temperature is above 0°C, which frequently results in a wet surface.[27] TOW is, therefore, a useful indicator of atmospheric corrosivity since a high TOW would imply a long-lasting effect of the electrolyte on the metal surface.

2.3 | Corrosion product characterisation

The Zeiss Merlin scanning electron microscope (SEM) with an energy dispersive X-ray spectrometer (EDS) was used for examination of the surface morphology and the Bruker D2 Phaser XRD machine was used as a material characterisation tool. Loose rust deposits were collected from the outer corroded surface and typically in powdered form for XRD analysis. The diffractometer is equipped with a Cu X-ray tube and Lynxeye (1D mode) detector. The analysis was carried out from 10° to 60° with a step width of 0.03° and data were collected for 0.5 s at each step. The diffraction pattern of each sample was compared to a database containing reference patterns to identify the phases that are present.

3 | RESULTS

3.1 | Variation of climatic factors

From Figure 3, it is evident that RH was highest during the summer season (November 2018 and April 2019) for both the PL and MC locations. However, PL can be considered a dry region compared to MC, with an average RH value of 68% and always lower than MC during the whole exposure period. Furthermore, Figure 4 shows that precipitation was also lower at PL, with a marked increase for both regions on December 2018 and April 2019. A washing effect of the rain was likely to be significant during these periods, thereby preventing the accumulation of corrosion products that would otherwise hinder corrosion progression. Figure 5 shows that PL is a hotter region compared to MC. However, variation of temperature throughout the year is the same for both regions with the period January 2019 to March 2019 being the hottest.

Table 2 shows the average Cl^- and SO_2 deposition rates at each site, the TOW for MC and PL and their corresponding ISO categories. The SO_2 level is at the lowest category P_0 for all sites, even at FG, despite its proximity to a power station releasing SO_2 gases into the atmosphere. The Cl^- deposition rates vary significantly between the various sites. In PL, the highest salinity rate is 57.25 $mg\,m^{-2}\,day^{-1}$ at RG, which is close to the upper

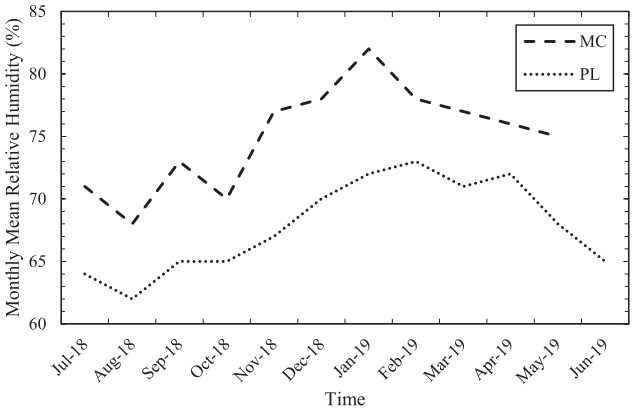

FIGURE 3 Mean relative humidity versus time for the Port Louis (PL) and Medine Camp de Masque (MC) locations[28]

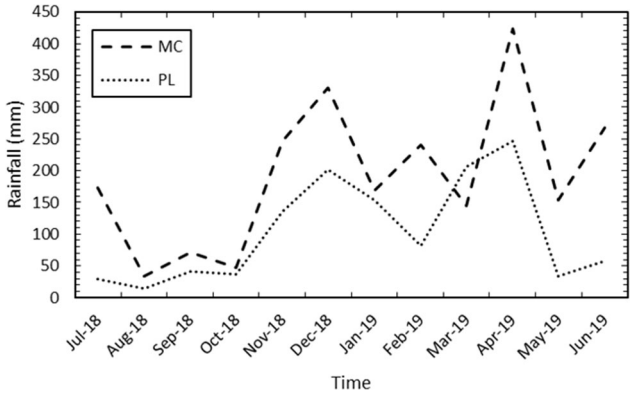

FIGURE 4 Rainfall versus time for the Port Louis (PL) and Medine Camp de Masque (MC) locations[28]

limit of 60 mg m^{-2} day^{-1} for the S_1 category ($3 < S \leq 60$). FG is in the mid-category while MA has a low value. The mid-island atmosphere (MC) has the highest TOW and a significant Cl^- content (higher than FG and MA). The latter confirms that variations in Cl^- deposition rate, as would be expected for a small island, cannot be differentiated by distance from the shoreline in this study. Factors such as the prevailing weather patterns and orography may predominately affect the Cl^- deposition rate around the island. In comparison, in an atmospheric corrosion study in the tropical climate of Ecuador, considered one of the most corrosive in South America, six atmospheric sites investigated in the marine zone of Manabí were categorised as being S_2 ($60 < S \leq 300$) with a TOW of 4889 h a^{-1}.[29] In another study in Male, the capital of the Maldives and a tropical island in the Indian Ocean, a high Cl^- deposition rate of S_3 ($300 < S \leq 1500$) was observed, with a TOW of 3067 h a^{-1}.[30]

3.2 | Visual appearance of corroded specimens

The colouration of rust layers varies with material, time and according to the corrosivity of the atmosphere.[14,31] Figures 6 and 7 show the marked differences in colour/texture of the skyward faces of plates exposed at FG, MA, RG (the three PL locations) and MC. Following the first removal after 2 months, the appearance of rusted carbon steel differs at the various locations, with notable orange and brown rust colours, consistent with the formation of lepidocrocite ($\gamma - FeOOH$) and goethite ($\alpha - FeOOH$) rust phases, respectively.[3,32–34] The orange colour at MC is strong evidence of the presence of lepidocrocite, which turns from orange to reddish-brown as the rust layer thickens.[35,36] The lighter colour of the rust at FG is characteristic of a saline environment and there is a uniform texture and colour on the top faces across all sites, with rougher surface textures observed for all the 11-month corroded plates due to extensive corrosion damage.[14] In contrast, the rear faces (shown in Figure 8) are of heterogeneous appearance, with a reddish-brown colour evident of the stable haematite phase ($\alpha - Fe_2O_3$),[33,37,38] and some dark/grey patches. The latter is an indication of the severity of corrosion on the groundward faces, which are not subjected to the washing effect of the rain and therefore have thicker rust layers.

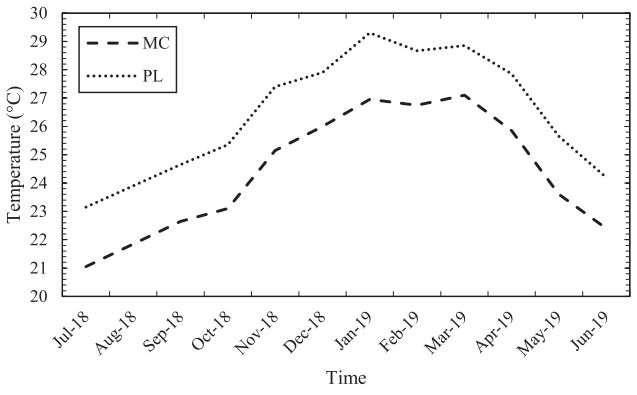

FIGURE 5 Mean temperature versus time for the Port Louis (PL) and Medine Camp de Masque (MC) locations[28]

3.3 | Variation of corrosion rate

The mass loss analysis was performed on metal plates subjected to 2, 5, 8 and at least 11 months of exposure such that the results are representative of the first year corrosion loss. The corrosion rate (r_{corr}) was calculated for each site at specific time intervals using Equation (1) and then substituted in Equation (2) to obtain the total attack (D). Table 3 lists the form of the power equation of D versus t and the corresponding b exponent and R^2 for each site. The value of b is suggestive of the corrosion products evolution; between 0.5 and 1.0 indicates a low protection performance of the corrosion layer, while less than 0.5 indicates corrosion product growth according to a parabolic function, due to corrosion products blocking aggressive species from reaching the underlying metal surface.[13] Therefore, based on the b value, the rust layer formed at each test site can be ranked from more protective to less protective in the following order: FG–RG–MA–MC.

TABLE 2 Assessment of environmental conditions at the three Port Louis locations and the MC site

Site	TOW (h a^{-1})	Cl^- level (mg m^{-2} day^{-1})	SO_2 level (mg m^{-2} day^{-1})	ISO 9223 Class TOW	Cl^-	SO_2
RG	1798	57.25	1.43 ± 0.54	τ_3 ($250 < \tau \leq 2500$)	S_1 ($3 < S \leq 60$)	P_0 ($P \leq 4$)
FG		41.56	1.90 ± 0.09			
MA		14.49	1.36 ± 0.33			
MC	3272	51.37	1.55 ± 0.54	τ_4 ($250 < \tau \leq 5500$)		

Abbreviations: FG, Fort George; MA, Mutual Aid; MC, Medine Camp de Masque; RG, Rajiv Gandhi; TOW, time-of-wetness.

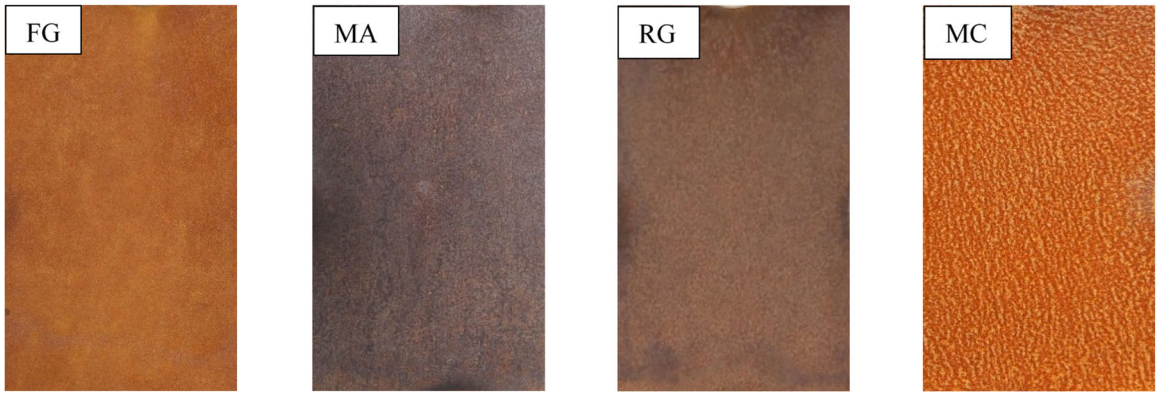

FIGURE 6 Two-month exposed skyward surfaces (from left to right: FG, MA, RG and MC). Dimensions: 150 × 100 mm. FG, Fort George; MA, Mutual Aid; MC, Medine Camp de Masque; RG, Rajiv Gandhi [Color figure can be viewed at wileyonlinelibrary.com]

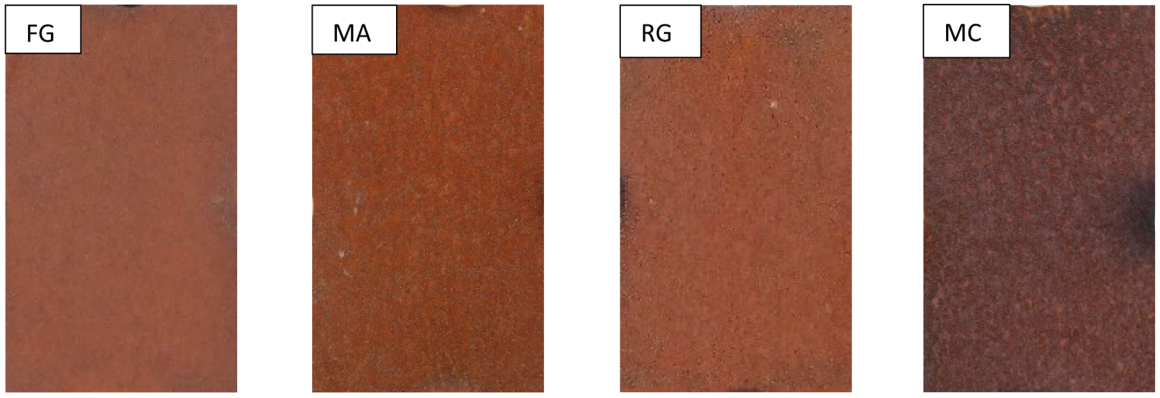

FIGURE 7 Eleven-month exposed skyward surfaces (from left to right: FG, MA, RG and MC). Dimensions: 150 × 100 mm. FG, Fort George; MA, Mutual Aid; MC, Medine Camp de Masque; RG, Rajiv Gandhi [Color figure can be viewed at wileyonlinelibrary.com]

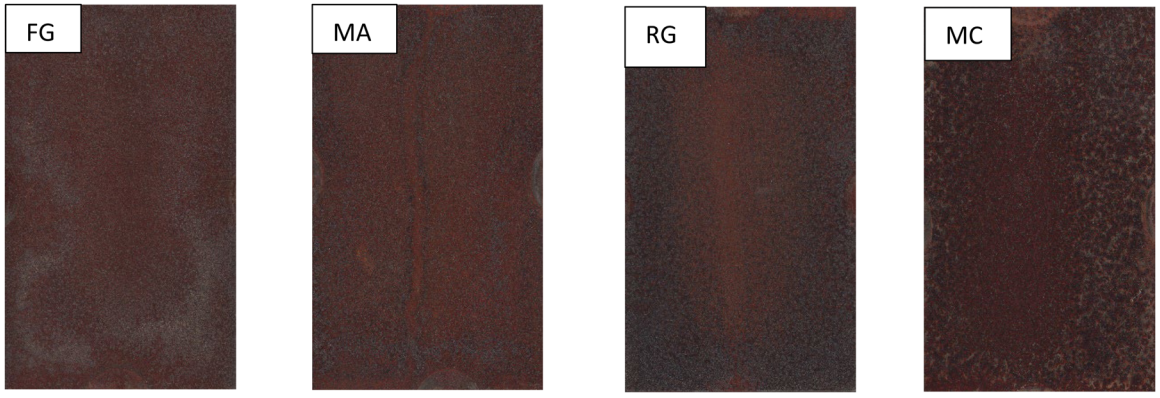

FIGURE 8 Eleven-month exposed groundward surfaces (from left to right: FG, MA, RG and MC). Dimensions: 150 × 100 mm. FG, Fort George; MA, Mutual Aid; MC, Medine Camp de Masque; RG, Rajiv Gandhi [Color figure can be viewed at wileyonlinelibrary.com]

Table 4 shows the yearly corrosion rates, as calculated using Equation (1), for the different test sites and the corresponding corrosivity categories as per ISO 9223.[27] All sites, apart from MC, are in the C2 category that represents low corrosivity. Overall, a broad range of corrosion rates are associated with the C2 category, that is, between 10 and 200 $g\,m^{-2}\,a^{-1}$. In the present study, the lowest corrosion rate is 77.6 $g\,m^{-2}\,a^{-1}$ and the highest being 189 $g\,m^{-2}\,a^{-1}$, is close to the upper limit for this category.

Figure 9 (D vs. t) shows that the data fits a linear function very well for all sites, except FG where the

TABLE 3 Mass loss data at the three Port Louis locations and the MC site

Site	Time interval (days)				Mass loss (g)				Equation	R^2
	1st	2nd	3rd	4th	1st	2nd	3rd	4th		
MA	66.9	151.9	243.76	348.83	1.16	1.55	1.90	2.33	$D = 51.04t^{0.4162}$	0.99
MC	65.6	155.6	246.03	346.01	2.47	3.86	5.10	6.82	$D = 148.77t^{0.5972}$	0.99
RG	61.9	153.9	245.89	350.93	1.75	2.48	2.92	3.65	$D = 79.35t^{0.4092}$	0.99
FG	61.8	152.7	244.66	349.78	3.10	4.83	5.07	5.70	$D = 132.26t^{0.3452}$	0.92

Abbreviations: FG, Fort George; MA, Mutual Aid; MC, Medine Camp de Masque; RG, Rajiv Gandhi.

TABLE 4 Corrosion kinetics at the three Port Louis locations and the MC site

Site	Total exposure (years)	Mass loss (g)	r_{corr} (g m^{-2} a^{-1})	Corrosivity category
MA	0.9531	2.33	77.6	C2
MC	0.9454	6.82	229	C3
RG	0.9588	3.65	121	C2
FG	0.9557	5.70	189	C2

Abbreviations: FG, Fort George; MA, Mutual Aid; MC, Medine Camp de Masque; RG, Rajiv Gandhi.

power-law function shown in Table 3 is favoured. There is a marked corrosion loss in the first few months of exposure at FG, followed by a decrease in corrosion rate until the end of the exposure period. This suggests that a coherent corrosion product layer forms rapidly, hindering further permeation of aggressive species to the underlying metal surface with time. Whereas at RG, MA and MC, the corrosion rate (D/t) is lower after two months, but then remains constant until the end of exposure indicating that the rust layer was a more porous/permeable barrier and the underlying steel substrate remained exposed. Given the urban environmental conditions at MA, effects of NO_x (mainly originating from vehicle emissions) predominate.[39] However, the latter show little involvement in accelerating the corrosion of carbon steel in this area, with a low mass loss at the first removal and subsequently a low corrosion rate. Due to a high TOW at MC, the reduced species can penetrate the permeable rust layer easily. There most probably is the formation of soluble corrosion products, which do not interfere with redox reactions (Equations 3 and 4) occurring in the wet/dry cycles, as corrosion proceeds faster.

$$Fe \rightarrow Fe^{2+} + 2e^{-}, \quad (3)$$

$$O_2 + 2H_2O + 4e^{-} \rightarrow 4OH^{-}. \quad (4)$$

3.4 | SEM/XRD

The specific rust phases that form in the diverse environmental conditions are also highly indicative of atmospheric corrosivity. Considering the main rust phases (lepidocrocite, goethite, magnetite and akaganeite), the strongest peaks from the XRD spectra shown in Figure 10 relate to the goethite and lepidocrocite phases. Magnetite (Fe_3O_4) and akaganeite ($\beta - FeOOH$) are present, but in small quantities, as observed from the small peaks. Jarosite—$KFe_3(OH)_6(SO_4)_2$, rozenite ($FeSO_4 \cdot 4H_2O$) and melanterite ($FeSO_4 \cdot 7H_2O$) can also be observed from the XRD spectra, confirming the presence of sulphate.[40,41] While most of the corrosion product surface morphologies were straightforward to identify and were just various forms of lepidocrocite and goethite (Figure 11), there were some unique morphologies of the minor constituent phases (not reported in previous studies). They were mainly globular and tubular formations, which are features of adherent rust.[38]

Lepidocrocite appeared as sandy crystals, bird's nests (Figure 11a), flowery structures with thin laminas or petals and clumps of grass structure (Figure 11b). At all four sites, goethite occurred as whiskers forming on the periphery of globules (Figure 11c) and bar-shaped laminar structures with thorny appearance (Figure 11d). The spinel form of magnetite occurred as a black sphere or crystal-like formations with isolated areas of a whitish colour (Figure 11e,f). Akaganeite was also found in various tubular formations (cigar-shaped) as shown in Figure 11g,h. Lath structures, typical of jarosite morphology, could be observed at FG as the EDS spectrum also shows significant potassium and sulphur content (Figure 12). At RG and MA, bird's nest and flowery crystals formed in circular nets. The latter was quite distant apart, with a relatively smooth surface at MA and a noticeable percentage of Cl^- and sulphur as shown in the EDS spectrum (Figure 13). The formation of surface cracks, observed from the SEM images, is due to the use

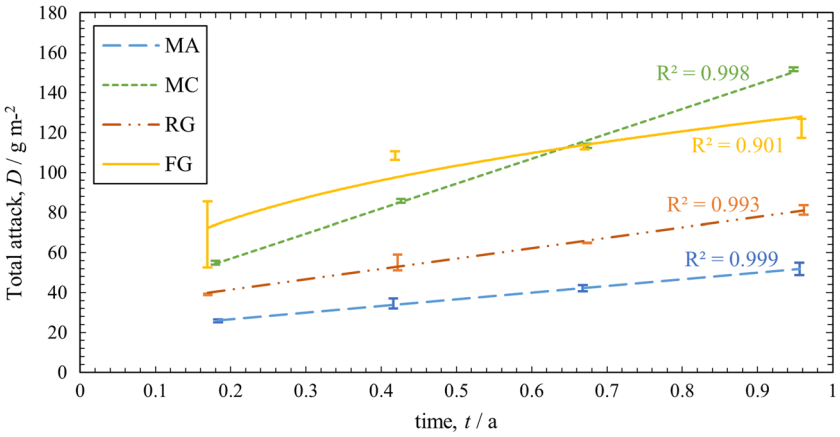

FIGURE 9 Comparison of corrosion performance, total attack (the degree of corrosion) versus time [Color figure can be viewed at wileyonlinelibrary.com]

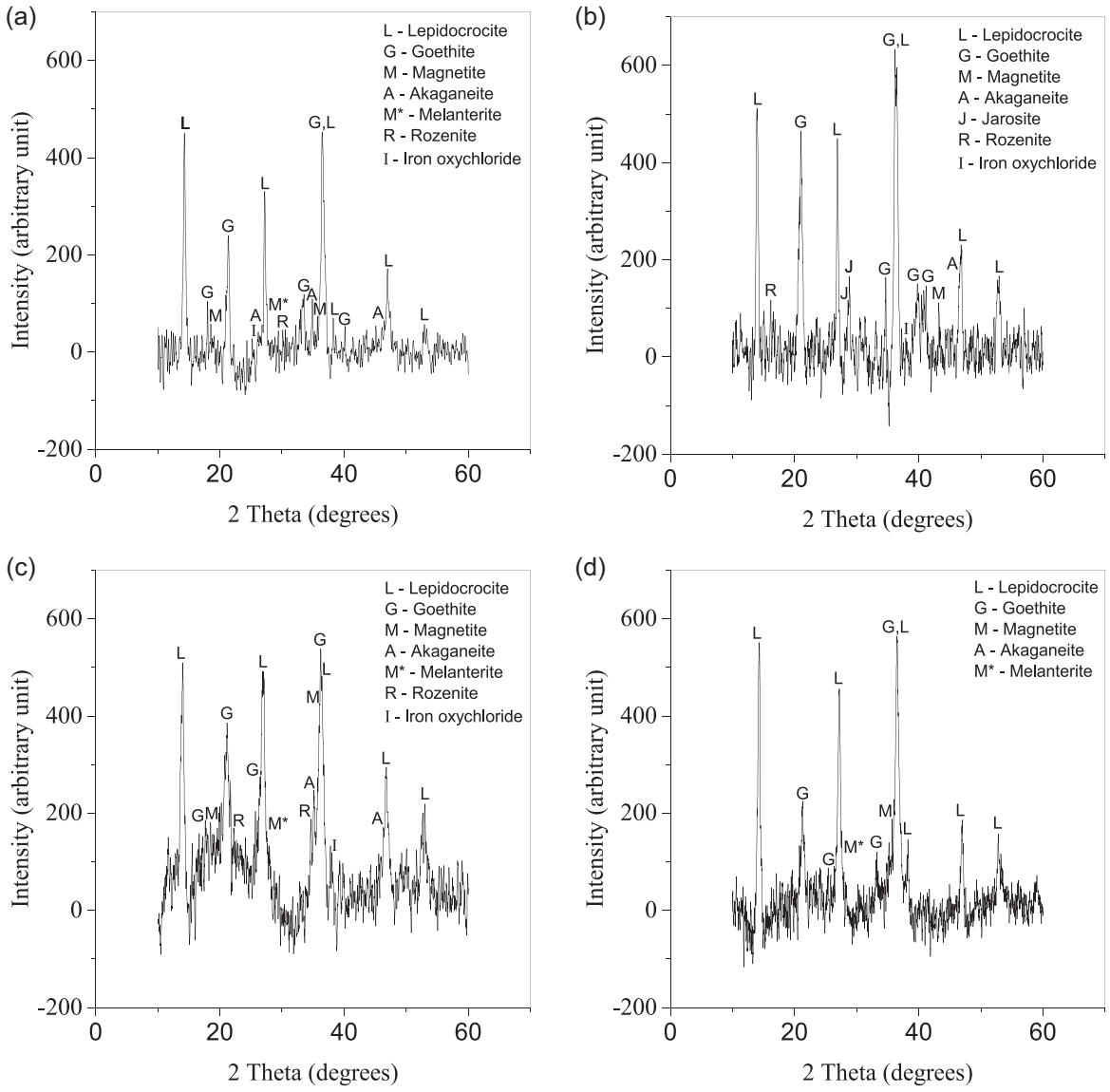

FIGURE 10 X-ray diffraction spectra for 11-month exposure at (a) Rajiv Gandhi, (b) Fort George, (c) Mutual Aid and (d) Medine Camp de Masque

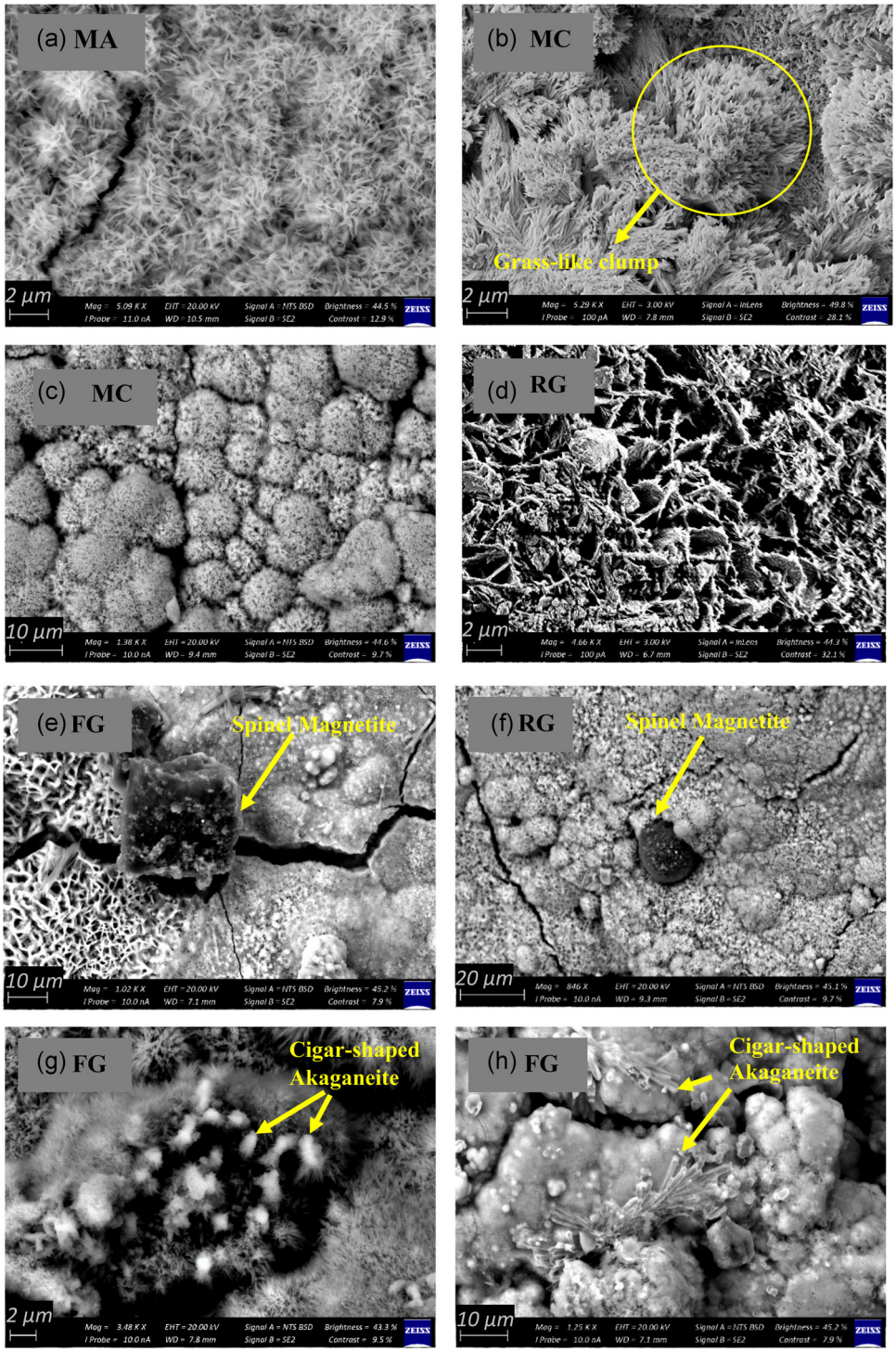

FIGURE 11 Corrosion product surface morphologies after an 11-month exposure at the three Port Louis locations and the Medine Camp de Masque (MC) site: (a, b) lepidocrocite, (c, d) goethite, (e, f) magnetite, (g, h) akaganeite [Color figure can be viewed at wileyonlinelibrary.com]

of the ultrahigh vacuum SEM and is also a characteristic of the rust layer formed. The presence of cracks results in a less protective barrier to electrolyte flowing to the metal substrate, even with the accumulation of corrosion products on the surface.

4 | DISCUSSION

The atmospheric salt concentration is generally significant for a few hundred metres from the coast before a rapid decrease towards inland[14] and decreasing

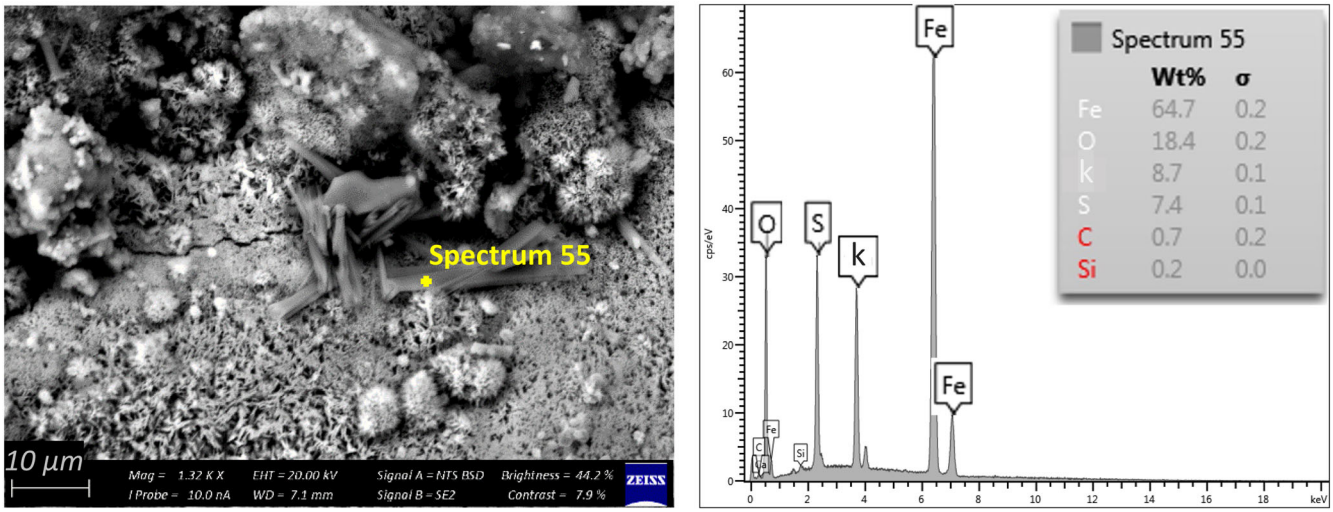

FIGURE 12 Jarosite morphology identified at Fort George from scanning electron microscope image and energy dispersive X-ray spectrometer spectrum [Color figure can be viewed at wileyonlinelibrary.com]

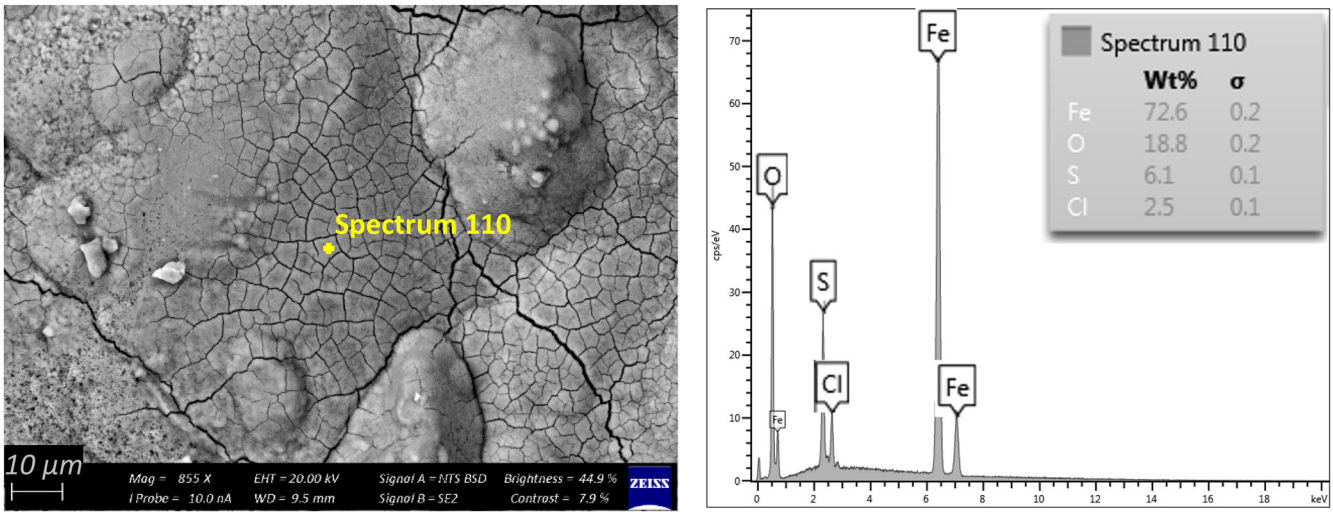

FIGURE 13 Elemental composition of the rust layer at Mutual Aid [Color figure can be viewed at wileyonlinelibrary.com]

corrosion kinetics with distance from the sea is usually observed.[8] However, the complex combination of location, exposed conditions, seasonality and the prevailing weather patterns can markedly affect the corrosion performance of bare S235 steel.[42] Figure 14 shows a plot of the wind speed versus time for PL and the average Cl^- deposition rates obtained from measurements carried out in the winter and summer. The Cl^- measurement periods coincide with the periods of high wind and low wind and the difference between the two sets of values is significant.

The wind direction in PL is generally west/north-west, that is, the wind direction is from land to sea. Therefore, the exposed specimen surfaces are facing the sea but on the downwind side. This explains the low Cl^- concentration at the various locations in PL, even when situated relatively close to the shoreline at FG. In this study, the mid-island atmosphere, MC, has a salinity level due to ocean generated sea aerosol,[43] which is higher than the two marine sites in PL: FG and MA. Therefore, the dependence of Cl^- deposition level solely based on distance from the shoreline is not correct given that locations close to the sea could result in lower corrosion rates than sites further inland, due to the complexity of chloride distribution in a marine-island atmosphere.[44] This has been reported in various studies, whereby influencing factors, such as obstacles and surface washing from rainwater have been noted.[21,45,46]

Furthermore, higher Cl^- deposition rate should not always be associated with a higher degree of corrosion since D can be higher in an atmosphere with lower salinity as shown in the graph of D versus Cl^- level (Figure 15a), plotted from the results obtained in the current study. Similarly, D does not necessarily increase with SO_2 level (Figure 15b). This implies that Cl^- and SO_2 do not primarily govern an increasing trend of corrosion acceleration within the regions investigated. For the present study, airborne salinity is relatively uniform from the coast to far inland, and RH is the only factor significantly different between PL and MC. The higher RH at MC leads to a predominance of the lepidocrocite rust phase at this site, as shown in the XRD spectrum (Figure 10), which reduces the protective capacity of the corrosion layer.[31,47,48] This is in agreement with the value of the power exponent b at MC, which is in the range 0.5–1.0, associated with low corrosion protection performance. FG, MA and RG have b values below this range, but closer to the threshold of 0.5, implying that deceleration of corrosion at these sites is not pronounced due to the porosity of the oxide film.

From Figure 9, a power relation between D and t is observed at FG. The power law is valid in cases of diffusion-controlled mechanisms, whereby the corrosion layer takes a consolidated form and species permeate through this layer to react with the steel substrate at the metal/rust interface.[1] In contrast, the rust layer within the first year of exposure at all the other sites grows at a constant rate, as shown by the linear D versus t relationship (Figure 9). Nevertheless, there is a significant difference between the corrosion rates of MA, RG and MC, which could be attributed to the different climatic conditions existing at the test locations. Fluctuations in RH and temperature give rise to the continuously repeating wetting and drying cycles, which influence the corrosion rate.[49] The type, rate of occurrence and length of these wet and dry periods have a noticeable effect on the constitution and morphology of the corrosion products formed on the metal surface. RH is known to increase corrosion rates and can be the main factor in low salinity and nonpolluted regions. MC is in the highest TOW category, with frequent condensation aided by the porous nature of the surface, causing metal surfaces to remain wet for a longer time. This explains the higher yearly corrosion rate obtained for this site. Furthermore, the formation of less adherent corrosion products such as lepidocrocite in high humidity conditions leads to enhanced diffusion of oxygen and water through the rust layer, which is in accordance with data obtained at other locations from previous studies in Mauritius.[50] However, there is no indication of any highly significant increase in corrosion kinetics during the most humid months for all sites.

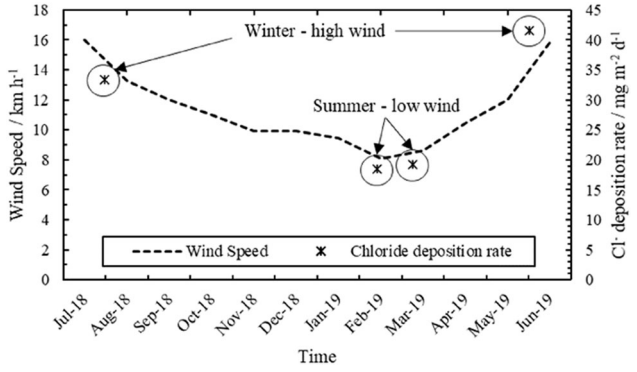

FIGURE 14 Effect of wind regime in Port Louis[28]

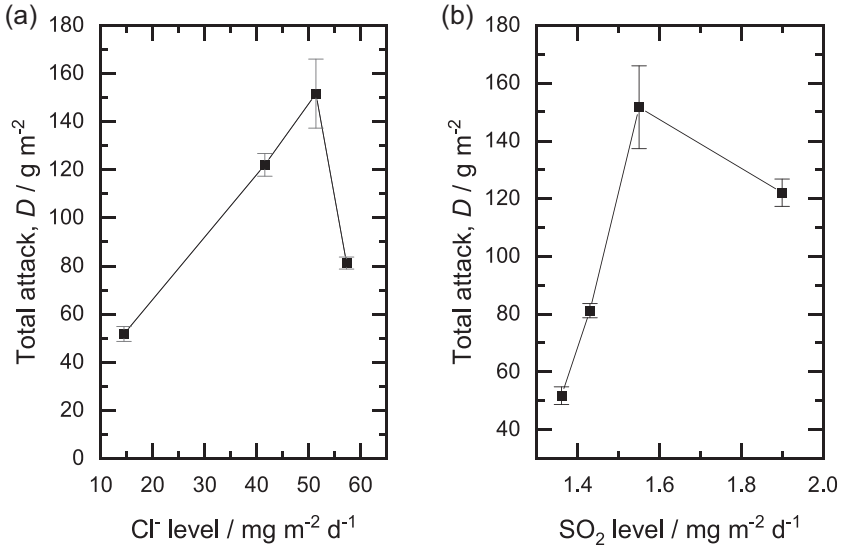

FIGURE 15 Effect of atmospheric pollutants on corrosion: (a) D versus Cl^- level and (b) D versus SO_2 level

Several factors, such as marine salts and gaseous pollutants may also contribute to an acceleration of the electrochemical process. Both Cl^- and SO_2 are major contributors to atmospheric corrosion.[21,39,51] SO_2 has also been found to have a more damaging effect on carbon steel than other metals such as copper.[39] In chloride-rich atmospheres, the presence of a salt solution on metal surfaces can cause condensation at a lower humidity level, which would otherwise occur at 100% RH.[52] Corrosion due to deliquescence of sea salt particles, mainly occurring as NaCl, deposited on metal surfaces is very common in marine atmospheres.[53] However, the RH of PL is below the deliquescence relative humidity (DRH) for NaCl (75%) and is, therefore, unable to induce deliquescence except for the minor constituents, such as $MgCl_2$ and $CaCl_2$ with lower DRHs of 33% and 20%, respectively.[54,55] Being hygroscopic, Cl^- and sulphate cause a prolonged TOW from an increase in moisture condensation. This explains the highest mass loss at FG in the first few months of exposure (Figure 9), due to a higher SO_2 concentration in the atmosphere at the nearby power station, leading to corrosivity that is nearly at the level of C3. The beginning of exposure coincides with the low rainfall period of the year (Figure 4), causing minimal washing off of pollutants deposited on the metal surface of FG. Nevertheless, it should be noted the SO_2 deposition measured at FG is low, despite being downwind of the power plant, due to the plume dispersing in the atmosphere without any significant deposition near ground level closer to the stack. Aggressive environments give rise to more protective rust phases, especially under moderate SO_2 conditions.[13] It is common to find sulphate as a constituent of the corrosion layer formed on exposure of steel to an industrial atmosphere.[2,3] Ferrous sulphate is likely to form if the SO_2 deposits are not washed off by rainwater. Given that the site at FG is very much exposed to precipitation, the influence of SO_2 is minimal and the enduring electrolyte on the metal surface causes the only sparse formation of ferrous sulphate in small pits.[56] The latter, if commonly present, leads to the rupture of even thicker corrosion layers formed in harsh atmospheres. It is known that sulphuric acid, which is an intermediate in the formation of ferrous sulphate from SO_2 (Equations 5 and 6), reappears again as constant contact with water causes further hydrolysis of ferrous sulphate, thereby causing continuous corrosion. In this study, the thin electrolyte layer on the metal surfaces exposed at the various sites undoubtedly comprises both Fe^{2+} and Fe^{3+} ions, in the form of metal complexes of iron bonded to water molecules and possibly to the Cl^- and sulphate ions present. This caused the precipitation of a small amount of the jarosite crystalline compound ($KFe_3(OH)_6(SO_4)_2$) at FG, due to the presence of potassium in the emissions from the burning of fuel in the heavy oil-fired power plant.

$$SO_2 + H_2O + 1/2O_2 \rightarrow H_2SO_4, \quad (5)$$

$$4H_2SO_4 + 4Fe + 2O_2 \rightarrow 4FeSO_4 + 4H_2O. \quad (6)$$

In addition, fragments of spinel magnetite were also found at FG. The latter shows a gradually decreasing corrosion rate after subsequent periods of exposure, indicating an increase in thickness of the rust layer, which reduces the contact of the underlying surface with electrolyte. This favours the oxidation of the existing rust phase instead, without an adequate supply of oxygen to keep the same rate of dissolution of metal ions. Nevertheless, the build-up of corrosion products with time would lead to the onset of cracks in the rust layer causing the corrosion rate to rise again.[50] This may lead to flaking of the outer rust layer, which is generally an agglomeration of crystalline phases, such as lepidocrocite and goethite. The residual rust layer is mainly amorphous FeOOH, which is compact and may contain magnetite and akaganeite. The latter forms under the significant presence of Cl^-, which acts as a catalyst in the process.[14] The presence of Cl^- increases the electrolyte conductivity, which may lead to the rupture of any protective layer.[21,31]

A time profile schematic for the evolution of corrosion products formation under the region effects is shown in Figure 16. Before exposure, the uncontaminated surface is covered with a passivating oxide or hydroxide layer of thickness in the order of a few nanometres. A few weeks later, a brown layer of lepidocrocite ($\gamma - FeOOH$) starts to appear, as an electrolyte film comprising of chlorides and sulphur dioxide from various sources sets on the metal surface. In the next stage of rust development, part of the lepidocrocite quickly transforms into the more stable goethite ($\alpha - FeOOH$) layer and the rusts grow as a porous membrane on the surface. The permeable rust layer, containing pores of up to 15 nm in diameter,[2] allows the ingress of pollutants-containing electrolytes to the substrate, causing corrosion to proceed at the same rate. This porous layer separating the substrate and the electrolyte is not able to prevent oxygen from migrating to the underlying steel, which also explains the absence of a consequent amount of the magnetite rust phase (Fe_3O_4). In the absence of oxygen, water becomes the oxidising agent in the formation of Fe_3O_4, in a reaction that also produces gaseous hydrogen (Equation 7).[57] Hence, the diffusion process is mainly absent in the corrosion occurring at the different sites, although to a lesser extent at FG. Chlorides in solution are attracted to Fe^{2+} being

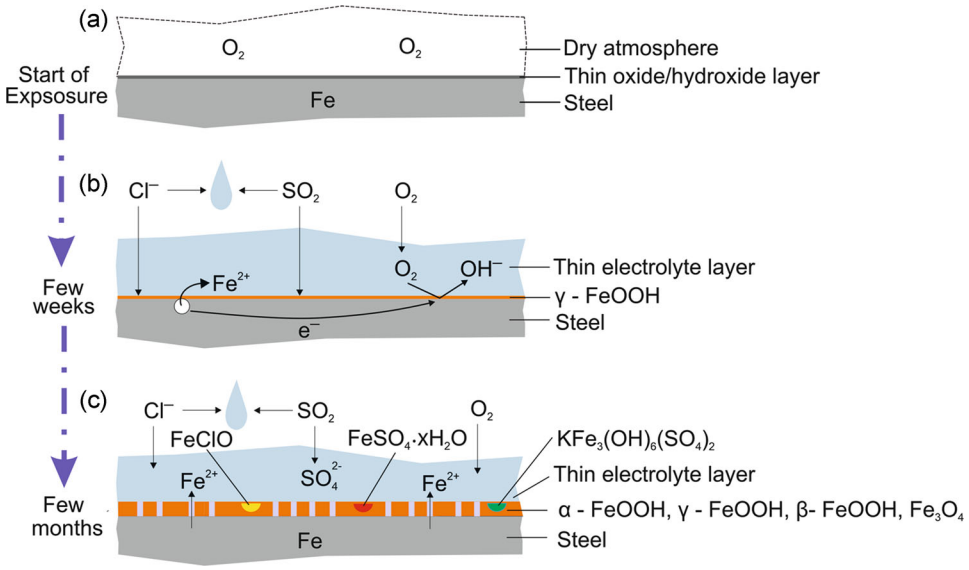

FIGURE 16 Evolution of corrosion product formation [Color figure can be viewed at wileyonlinelibrary.com]

released through the pores, possibly forming iron oxychlorides (FeClO), with chloride also leading to some akaganeite (β-FeOOH) formation. The latter is present in low percentages and, therefore, is not able to cause a significant rise in corrosion rate.

$$3Fe + 4H_2O \rightarrow Fe_3O_4 + H_2. \quad (7)$$

The Cl^- deposition rate is in the S_1 category for all regions, with a relatively higher deposition rate at RG (57.25 mg m^{-2} day^{-1}). The latter, being at a higher elevation than the other sites in PL, is situated at the foot of the Moka mountain range, which is likely to cause increased salt deposition due to favourable airflow patterns on the ridge slope.[58] Based on results from a corrosion study involving field exposures of carbon steel in Chile (nontropical) and Venezuela (tropical), there has been a rapid increase in corrosion rate beyond a Cl^- deposition rate of 50 mg m^{-2} day^{-1}; however, greater than 600 mm rain washes the Cl^- content of the surface, reducing the damage.[42] As shown in Figure 4, this rainfall threshold has not been attained at PL and MC. From the EDS spectrum in Figure 13, MA was the site with a clear presence of Cl^- and sulphate in the corrosion products (on the outer surface), although it has the lowest corrosion rate and Cl^- deposition level (14.49 mg m^{-2} day^{-1}). The presence of building infrastructure in the immediate environment and a narrow bay led to a reduced salinity level compared to the other sites.[59] Furthermore, the specimens are shielded from the effect of rain, which therefore does not contribute to the washing-off of chlorides or sulphates deposited on the surface of the metal. However, these particles do not penetrate the rust layer as there is insufficient sorption and precipitation for electrolyte formation, leaving a relatively dry metal surface.

Although at a slower rate compared to MC, the corrosion loss at MA and RG also increases linearly with time, indicating that the corrosion process persists during the yearlong exposure, and the rust layer is not protective. Due to the build-up of corrosion products, spalling of the rust or an increase in friability of the resulting fragments with time will mean that corrosion will accelerate. However, the fact that the first-year corrosion rate does not decrease for MC, MA and RG is a rare phenomenon, which is not observed in other studies. As per ISO 9223,[27] all locations in PL are of S_1P_0 environmental classification (Table 2) and C2 corrosivity category as determined from corrosion rate results (Table 4). Field exposures carried out in other countries with a similar atmosphere (S_1P_0), but not necessarily the same TOW, are listed in Table 5. Corrosivity categories within 'C2–C4' have been obtained for each of the 17 test stations of S_1P_0 category and high TOW (at least τ_4) in the Ibero-American area.[51] A location in Barranquilla (Columbia) has even been associated with the highest corrosivity category (C5) despite having such a low level of pollution.[13] In Venezuela, C3 or C4 has been associated with the S_1P_0 regions having a quite high TOW (τ_4).[42] However, low corrosivity (C2) has been observed in Campeche (Mexico), although the humidity is high.[60] Therefore, S_1P_0 regions are represented by a wide range of corrosion rates, which cannot be explained by differences in TOW. A previous study carried out in an S_1P_1 location in PL, lead to a C4 corrosivity classification.[50] Despite being situated on the seashore,

TABLE 5 Corrosivity of atmospheres in S_1P_0 category regions in tropical countries

Location	TOW	ISO 9223 corrosivity category
Campeche (Mexico)	τ_4	C2
Ibero American	τ_4, τ_5	C2–C4
Venezuela	τ_4	C3, C4
Barranquilla (Columbia)	τ_5	C5
Port Louis (Mauritius)	τ_3	C4

Abbreviation: TOW, time-of-wetness.

Cl^- deposition rate recorded at this site was much lower than the other sites investigated in the current study. However, the SO_2 level was relatively high, which could be the cause for the more corrosive atmosphere.

Research on marine atmospheric corrosion in tropical regions have attracted interest from several researchers through the years. Atmospheric corrosion tests were performed in the Caribbean area comprising of Cuba, Mexico and Venezuela, all with a maritime climate.[8] Pollutants released from factories and other sources did not have any noticeable effect on corrosion rate. Even with a higher Cl^- deposition level, sites closer to the sea may be less aggressive than sites further inland and highly humid. The results of field exposures in other regions in Mauritius showed that the corrosivity of the Mauritian atmosphere, in general, is at category C3, which was mainly attributed to the high RH and, hence, the high TOW prevailing around the island.[10] It should be noted that airborne salinity and SO_2 levels were low in the regions investigated. In general, pollution level remains low in Mauritius, apart from PL, especially closer to the power plants. In the current study, there is the formation of a rust layer in a marine atmosphere in which the airborne salinity is low. Coastal regions are known to cause higher corrosion rates;[14,23,45] however, this is not observed here.

5 | CONCLUSIONS

S235 carbon steel specimens were exposed at three specific locations (MA, RG and FG) in the marine industrial environment of PL and one mid-island rural atmosphere (MC) for a period of nearly 1 year. Key insights into the Mauritius marine atmospheric corrosion of carbon steel are as follows:

1. The atmospheric conditions at the four sites limited the formation of significant akaganeite and magnetite phases, which normally require high chloride and acidic contents. However, small amounts of these compounds are present and are not formed at the metal/rust interface under limited oxygen conditions.
2. Marked corrosion rate differences were observed at the three PL test sites, implying that location-specific conditions, such as proximity to heavy-oil fired power stations and natural or manmade forms, were having an influence on corrosion kinetics.
3. Despite its marine atmosphere, corrosion rates in PL are also dependent on wind direction. All three locations had chloride deposition rates in the S_1 category, attributable to the predominant wind direction from land to sea.
4. Chloride deposition rate at the PL sites was highly seasonal (roughly 19 and 37 $mg\,m^2\,day^{-1}$, for the summer and winter, respectively) and as such linked to wind speed. Thus, demonstrating airborne salinity was highly dependent on prevailing weather conditions.
5. At MC, the airborne salinity (51.4 $mg\,m^2\,d^{-1}$) was markedly higher than two of the PL sites, implying that significant chloride levels exist over the in-land regions of Mauritius.
6. The importance of RH in accelerating atmospheric corrosion has been highlighted, especially for small tropical islands such as Mauritius. The industrial marine sites in PL have demonstrated corrosion rates in the C2 category as opposed to the more humid central region associated with a higher corrosivity category.

ACKNOWLEDGEMENTS

The authors express their gratitude to the Central Electricity Board, Mauritius Civil Service Mutual Aid Association Ltd. and Rajiv Gandhi Science Centre for allocating the required space in their premises for the field tests. The authors would also like to thank the Mauritius Meteorological Services for providing the climatic data. This study received funding under the Africa Collaboration Grant to conduct X-ray diffraction analysis, scanning electron microscopy and energy-dispersive X-ray spectroscopy using equipment available at Stellenbosch University. Correction added on 4 April 2022, after first online publication: Online open access has been added. Open access funded by JISC - UNIVERSITY OF SOUTHAMPTON.

CONFLICTS OF INTEREST

The authors declare no conflicts of interest.

AUTHOR CONTRIBUTIONS

Yashwantraj Seechurn was involved in conceptualisation, methodology, investigation, funding acquisition, formal analysis, visualisation, writing—original draft,

review and editing. Baboo Y. R. Surnam and Julian A. Wharton were involved in supervision and writing—review and editing.

DATA AVAILABILITY STATEMENT

The data that support the findings of this study are available from the corresponding author upon reasonable request.

ORCID

Yashwantraj Seechurn http://orcid.org/0000-0002-1733-0642
Baboo Y. R. Surnam http://orcid.org/0000-0002-3941-8135
Julian A. Wharton http://orcid.org/0000-0002-3439-017X

REFERENCES

[1] M. Morcillo, B. Chico, J. Alcántara, I. Díaz, J. Simancas, D. De La Fuente, *Mater. Corros.* **2015**, *66*, 882.
[2] C.L. Wallin, J. Tidblad, T. E. Graedel, *Atmospheric Corrosion*, John Wiley & Sons, Inc., Hoboken, NJ **2016**.
[3] B. Jegdic, S. Polic-Radovanovic, S. S. Ristic, A. B. Alil, *Sci. Tech.* **2011**, *61*, 50.
[4] Mauritius Meteorological Services, Climate of Mauritius, http://metservice.intnet.mu/climate-services/climate-of-mauritius.php (accessed: June 2021).
[5] CEB, power stations, https://ceb.mu/our-activities/power-stations accessed: June 2021.
[6] P. Tatayah, Air quality—Fort George, Mauritius, **2017**.
[7] J. F. Ríos Rojas, D. Escobar Ocampo, E. A. Hernández García, C. E. Arroyave Posada, *DYNA.* **2015**, *82*, 128.
[8] F. Corvo, C. Haces, N. Betancourt, L. Maldonado, L. Véleva, M. Echeverria, O. T. De Rincón, A. Rincón, *Corros. Sci.* **1997**, *39*, 823.
[9] C. G. Staub, F. R. Stevens, P. R. Waylen, *Appl. Geogr.* **2014**, *54*, 222.
[10] B. Y. R. Surnam, C. V. Oleti, *Corros. Eng. Sci. Technol.* **2012**, *47*, 446.
[11] Y. Liu, Z. Wang, Y. Wei, *Int. J. Electrochem. Sci.* **2019**, *14*, 1147.
[12] S. W. Dean, G. Hernandez-duque, J. B. Bushman, *Marine Corrosion in Tropical Environments*, ASTM, West Conshohocken, PA **2000**.
[13] J. G. Castaño, C. A. Botero, A. H. Restrepo, E. A. Agudelo, E. Correa, F. Echeverría, *Corros. Sci.* **2010**, *52*, 216.
[14] J. Alcántara, B. Chico, I. Díaz, D. de la Fuente, M. Morcillo, *Corros. Sci.* **2015**, *97*, 74.
[15] A. Gismelseed, S. H. Al-Harthi, M. Elzain, A. D. Al-Rawas, A. Yousif, S. Al-Saadi, I. Al-Omari, H. Widatallah, K. Bouziane, *Hyperfine Interact.* **2006**, *167*, 753.
[16] A. Taalba, H. Xie, M. G. Scarratt, S. Bélanger, M. Levasseur, *Biogeosciences* **2013**, *10*, 6793.
[17] *BS EN ISO 9225*, Corrosion of metals and alloys—Corrosivity of atmospheres—Measurement of environmental parameters, BSI Standards Limited **2012**.
[18] *ISO 8565*, Metals and alloys—Atmospheric corrosion testing—General requirements **2011**.
[19] *BS EN ISO 8407*, Corrosion of metals and alloys—Removal of corrosion products from corrosion test specimens, BSI Standards Limited **2014**.
[20] *BS EN ISO 9226*, Corrosion of Metals and Alloys—Corrosivity of atmospheres - Determination of corrosion rate of standard specimens for the evaluation of corrosivity, BSI Standards Limited **2012**.
[21] S. Sabir, A. A. Ibrahim, *Corros. Eng. Sci. Technol.* **2017**, *52*, 276.
[22] *BS EN ISO 9224*, Corrosion of metals and alloys—Corrosivity of atmospheres—Guidance values for the corrosvity categories, BSI Standards Limited, **2012**.
[23] M. Benarie, F. L. Lipfert, *Atmos. Environ.* **1986**, *20*, 1947.
[24] Q. Yu, C. Fang Dong, Y. Hua Fang, K. Xiao, C. Yun Guo, G. He, X. Gang Li, *J. Iron Steel Res. Int.* **2016**, *23*, 1061.
[25] D. de la Fuente, I. Díaz, J. Simancas, B. Chico, M. Morcillo, *Corros. Sci.* **2011**, *53*, 604.
[26] Y. Ma, Y. Li, F. Wang, *Corros. Sci.* **2010**, *52*, 1796.
[27] *BS EN ISO 9223*, Corrosion of metals and alloys—Corrosivity of atmospheres—Classification, determination and estimation, BSI Standards Limited **2012**.
[28] Mauritius Meteorological Services, Meteorological Observations and Climatological Summaries **2019**. http://metservice.intnet.mu/publication.php (accessed: June 2021).
[29] J. C. Guerra, A. Castañeda, F. Corvo, J. J. Howland, J. Rodríguez, *Mater. Corros.* **2019**, *70*, 444.
[30] W. Wu, X. Cheng, J. Zhao, X. Li, *Corros. Sci.* **2020**, *165*, 108416.
[31] J. Alcántara, de la D. Fuente, B. Chico, J. Simancas, I. Díaz, M. Morcillo, *Mater. (Basel)* **2017**, *10*, 406.
[32] H. Tamura, *Corros. Sci.* **2008**, *50*, 1872.
[33] A. Momber, *Mater. Corros.* **2012**, *63*, 333.
[34] A. C. Scheinost, U. Schwertmann, *Soil Sci. Soc. Am. J.* **1999**, *63*, 1463.
[35] J. F. W. Bowles, *Encycl. Geol* **2021**, 442.
[36] R. Balasubramaniam, A. V. R. Kumar, P. Dillmann, *Sci. Archaeol. Archaeomaterials* **2005**, *85*, 275.
[37] J. Alcántara, B. Chico, J. Simancas, I. Díaz, D. de la Fuente, M. Morcillo, *Mater. Charact.* **2016**, *118*, 65.
[38] M. Morcillo, B. Chico, J. Alcántara, I. Díaz, R. Wolthuis, D. de la Fuente, *J. Electrochem. Soc.* **2016**, *163*, C426.
[39] K. Kreislova, D. Knotkova, *Mater. (Basel)* **2017**, *10*, 394.
[40] T. E. Graedel, *J. Electrochem. Soc.* **1990**, *137*, 2385.
[41] U. Schwertmann, R. M. Cornell, *Iron oxides in the laboratory, preparation and characterization, WILEY-VCH Verlag GmbH*, Federal Republic of Germany, Weinheim **1992**.
[42] R. Vera, O. T. de Rincón, M. Bagnara, N. Romero, R. Araya, S. Ossandón, *Mater. Corros.* **2018**, *69*, 614.
[43] I. S. Cole, D. A. Paterson, W. D. Ganther, *Corros. Eng. Sci. Technol.* **2003**, *38*, 129.
[44] G. R. Meira, C. Andrade, C. Alonso, I. J. Padaratz, J. C. Borba, *Corros. Sci.* **2008**, *50*, 2724.
[45] F. Corvo, T. Perez, L. R. Dzib, Y. Martin, A. Castañeda, E. Gonzalez, J. Perez, *Corros. Sci.* **2008**, *50*, 220.
[46] S. Pintos, N. V. Queipo, O. Troconis De Rincón, A. Rincón, M. Morcillo, *Corros. Sci.* **2000**, *42*, 35.
[47] S. Hœrlé, F. Mazaudier, P. Dillmann, G. Santarini, *Corros. Sci.* **2004**, *46*, 1431.

[48] H. Antony, L. Legrand, L. Maréchal, S. Perrin, P. Dillmann, A. Chaussé, *Electrochim. Acta* **2005**, *51*, 745.
[49] C. G. Soares, Y. Garbatov, A. Zayed, G. Wang, *Corros. Sci.* **2014**, 51.
[50] B. Y. R. Surnam, *Anti-Corrosion Methods Mater* **2015**, *62*, 246.
[51] E. Almeida, M. Morcillo, B. Rosales, *Mater. Corros.* **2000**, *51*, 865.
[52] D. Landolt, *Corrosion and surface chemistry of metals*, EPFL Press, Lausanne, Switzerland **2007**.
[53] I. S. Cole, D. Lau, D. A. Paterson, *Corros. Eng. Sci. Technol.* **2004**, *39*, 209.
[54] R. M. Katona, J. C. Carpenter, A. W. Knight, C. R. Bryan, R. F. Schaller, R. G. Kelly, E. J. Schindelholz, *Corros. Sci.* **2020**, *177*, 108935.
[55] E. Schindelholz, R. G. Kelly, *Corros. Rev.* **2012**, *30*, 135.
[56] I. Matsushima, in *Uhlig's Corrosion Handbook* (Ed: R. W. Revie), John Wiley & Sons, Inc., Hoboken, NJ **2011**.
[57] D. De La Fuente, I. Díaz, J. Alcántara, B. Chico, J. Simancas, I. Llorente, A. García-Delgado, J. A. Jiménez, P. Adeva, M. Morcillo, *Mater. Corros.* **2016**, *67*, 227.
[58] I. S. Cole, W. D. Ganther, D. A. Paterson, G. A. King, S. A. Furman, D. Lau, *Corros. Eng. Sci. Technol.* **2003**, *38*, 259.
[59] I. S. Cole, D. A. Paterson, W. D. Ganther, A. Neufeld, B. Hinton, G. McAdam, M. McGeachie, R. Jeffery, L. Chotimongkol, C. Bhamornsut, N. V. Hue, S. Purwadaria, *Corros. Eng. Sci. Technol.* **2003**, *38*, 267.
[60] D. C. Cook, A. C. Van Orden, J. J. Carpio, S. J. Oh, *Hyperfine Interact.* **1998**, *113*, 319.

SUPPORTING INFORMATION

Additional supporting information may be found in the online version of the article at the publisher's website.

How to cite this article: Y. Seechurn, B. Y. R. Surnam, J. A. Wharton, *Mater. Corros.* **2022**;73:1474–1489.
https://doi.org/10.1002/maco.202112871